RAA 2021 Vol. **21** No. **10**, 268(11pp) doi:10.1088/1674-4527/21/10/268

http://www.raa-journal.org *http://iopscience.iop.org/raa*

Research in Astronomy and Astrophysics

Research on performances of back-illuminated scientific CMOS for astronomical observations

Peng Qiu[1,2], Yong Zhao[1,2], Jie Zheng[1], Jian-Feng Wang[1] and Xiao-Jun Jiang[1,2]

[1] CAS Key Laboratory of Optical Astronomy, National Astronomical Observatories, Chinese Academy of Science, Beijing 100101, China; *pqiu@nao.cas.cn*

[2] School of Astronomy and Space Science, University of Chinese Academy of Sciences, Beijing 100049, China

Received 2020 July 14; accepted 2021 June 28

Abstract To evaluate performances of a back-illuminated scientific CMOS (sCMOS) camera for astronomical observations, comparison tests between Andor Marana sCMOS and Andor iKon-L 936 CCD cameras were conducted in a laboratory and on a telescope. The laboratory tests showed that the readout noise of the sCMOS camera is about half lower, the dark current is about 17 times higher, the dynamic range is lower in the 12-bit setting and higher in the 16-bit setting, and the linearity and bias stability are comparable relative to those of the CCD camera. In field tests, we observed the open cluster M67 with the sCMOS and CCD cameras on a 60 cm telescope. Unlike the CCD camera, the sCMOS camera has a dual-amplifier architecture. Since a 16-bit image of the sCMOS camera is composed of two 12-bit images sampled with 12-bit high gain and low gain amplifiers simultaneously, it is not real 16-bit output data. The evaluation tests indicated that the dual-amplifier architecture of the sCMOS camera leads to a decline of photometric stability by about six times around specific pixel counts. For photometry of bright objects with similar magnitudes that require high frame rates, the sCMOS camera under 12-bit setting is a good choice. Therefore, the sCMOS camera is fitted with survey observations of variable objects requiring short exposure times, mostly less than 1 s, and high frame rates. It also satisfies the requirements for an offset guiding instrument owing to its high sensitivity, high temporal resolution and high stability.

Key words: detectors — photometric — observational

1 INTRODUCTION

Both CMOS and CCD sensors emerged as digital devices with advanced technologies in the 1960s. Due to its complicated structure, the CMOS sensor did not demonstrate sufficiently good performance as a photosensitive sensor at the beginning. In the late 1990s, with development of phone cameras and industrial cameras, the CMOS sensor has seen a boost[1]. In civilian fields, CMOS sensors have been replaced by CCD sensors and become the most-used image sensors at present. However, the CCD sensor is still dominant in astronomical observations.

In 2009, a technology of scientific CMOS (sCMOS) was developed and equipped with Andor Technology PLC Neo sCMOS camera, which has a science-grade front-illuminated (FI) sensor with a pixel size of 6.5 micrometers, a resolution of 2560×2160, a peak quantum efficiency (QE) of about 60% at 580 nm and a fill factor of around 90%. The Neo sCMOS camera had been evaluated for fast photometry by Qiu et al. (2013).

The scientific backside illuminated (BSI) sensor GSENSE400BSI was developed for scientific applications (Ma et al. 2015). Compared with the FI image sensor, the BSI image sensor has a higher fill factor and QE, which can significantly improve observational efficiencies in astronomy. The first scientific BSI camera Marana sCMOS camera produced by Andor in August 2018 was designed explicitly for astronomy and physical sciences using the GSENSE400BSI image sensor, which has a pixel size of 11 micrometers, a large format of 2048×2048, a peak QE of about 95% at 560 nm, a 100% fill factor, a high frame rate of 24 fps and a readout noise (RN) of 2 e^-. Judging from the specifications given in the factory report, this camera has an outstanding performance. Although the low RN, high frame rate, high QE and electronic shutter of the Marana sCMOS camera are essential for astronomical

[1] https://andor.oxinst.com/learning/view/article/the-history-and-development-of-scmos

Fig. 1 Two cameras we tested. The Andor Marana sCMOS camera (*left*) and the Andor iKon-L 936 CCD camera (*right*).

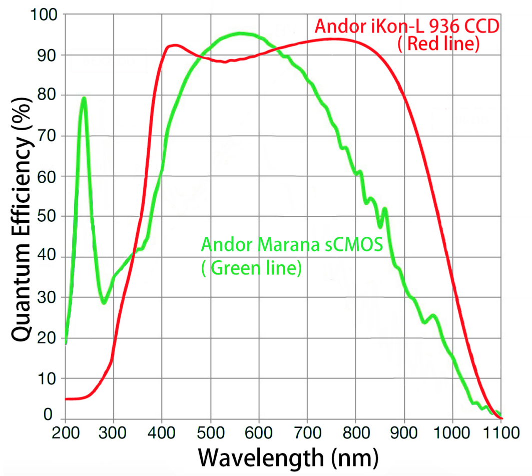

Fig. 2 Wavelength dependences of QEs of the Marana sCMOS and iKon-L 936 CCD cameras.

observations, it has not been tested for astronomical usage yet. Therefore, we evaluated the performance of the Marana sCMOS camera in comparison to the Andor iKon-L 936 CCD camera in an optical laboratory and on a 60 cm f/4.23 telescope.

We will introduce the specifications of Marana sCMOS and iKon-L 936 CCD in Section 2. Results of the laboratory tests will be presented in Section 3. Results of the field tests will be presented in Section 4. The conclusion will be described in Section 5.

2 SPECIFICATIONS OF CAMERAS

Pictures of the two cameras we tested, Andor Marana sCMOS and Andor iKon-L 936 CCD, are displayed in Figure 1, both of which are scientific BSI cameras with a 100% fill factor. The iKon-L 936 CCD camera is chosen to conduct a comparative test because it has been widely utilized in astronomical observations. This CCD camera is used in astronomy observations on the 60 cm, 85 cm, 1 m and 2.16 m telescopes at Xinglong Observatory, National Astronomical Observatories, Chinese Academy of Sciences (NAOC).

The specifications given in the manufacturers' datasheets are summarized in Figure 2 and Table 1[2].

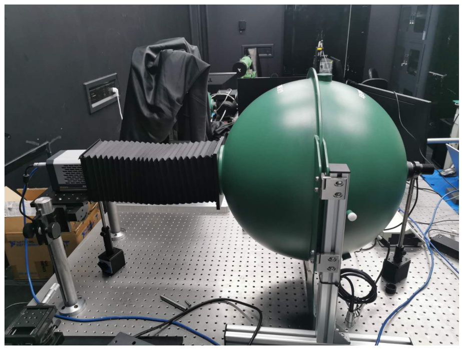

Fig. 3 Set up of test platform in an optical dark room.

Both cameras have high QEs, above 90% at peak, good linearities, a 100% fill factor and the same format of 2048×2048, but different pixel sizes of 11 and 13.5 micrometers. Compared with a CCD camera, an sCMOS camera has a higher readout rate, higher frame rate and lower RN, but higher dark current.

Because the sCMOS camera incorporates an electronic shutter in the sensor but the CCD camera is equipped with a mechanical shutter, it does not need to consider the shutter effect in astronomical observations with a short exposure time. Considering the high dark current, high frame rate and low RN, the sCMOS camera might be more suitable for high temporal resolution astronomical observations.

The sCMOS camera has configurations of 12-bit and 16-bit data formats. The CCD camera operates with readout modes with combinations of readout rates of 0.05 MHz, 1 MHz, 3 MHz and 5 MHz and three preamplifier modes of 1×, 2× and 4×. The 1 MHz 2× and 4× settings of the iKon-L 936 CCD camera are regularly applied in astronomical observations to balance its frame rate and RN. Aimed at studying the performances of the sCMOS camera for photometry, we conducted the following comparative tests in the two typical settings of the sCMOS camera and the 1 MHz 2× and 4× settings of the CCD camera in the laboratory tests and field tests.

3 LABORATORY TESTS

We conducted a series of laboratory tests on the performances of the two cameras, including RN, gain, full well capacity (FWC), bias, pixel uniformity, linearity, dark current and dynamic range.

[2] Data and QE curves describing Andor Marana sCMOS and iKon-L 936 CCD cameras in Fig. 2 and Table 1 are from the manufacturers' datasheets: *https://andor.oxinst.com/products/scmos-camera-series/marana-scmos* and *https://andor.oxinst.com/products/ikon-xl-and-ikon-large-ccd-series/ikon-l-936*.

Table 1 Specifications of the Cameras in Data Sheet Provided From Manufacturers

Camera	Marana sCMOS	iKon-L 936 CCD
Type	scientific BSI	scientific BSI
Active pixels	2048×2048	2048×2048
Pixel size (μm)	11×11	13.5×13.5
Sensor size (mm)	22.5×22.5	27.6×27.6
Shutter	electronic shutter	mechanical shutter
Readout rate	100/200 MHz	0.05/1/3/5 MHz
RN (e^-, typical)	1.6	2.9@0.05 MHz, 7.0@1 MHz, 11.7@3 MHz, 31.5@5 MHz
Frame rate	24@100 MHz, 48@200 MHz	0.011@0.05 MHz, 0.221@1 MHz, 0.607@3 MHz, 0.953@5 MHz
Pixel well depth (e^-, typical)	85 000	150 000
Cooling	-25° C (@30° C) -45° C (@10° C)	-80° C (@25° C)
Dark current (e^- pix^{-1} s^{-1},typical)	0.4 @ -25° C 0.2 @ -45° C	0.006 @ -80° C
Linearity	>99.7 %	>99 %
Fill factor	100 %	100 %
Peak QE (typical)	95 % @ 570 nm	93 % @ 750 nm

3.1 Gain, RN and FWC

The gain, RN and FWC are derived from a photon transfer curve (PTC) (Janesick 2007), which is based on two bias images taken under dark conditions in the optical laboratory with an exposure time of zero seconds. We obtained a series of image data with an integrating sphere and a stable light source by increasing exposure time until the images reached saturation and relied on a pair of two frames with the same exposure time.

We set up a testing system on a platform in the optical laboratory as illustrated in Figure 3. The stable light source is produced from the Thorlabs Inc M590L3. The nominal wavelength of the M590L3 is 590 nm with a bandwidth (full width at half maximum, FWHM) of 18 nm. The diameter of a detection port of the integrating sphere is around 10 cm. In order to get stable and uniform light, the distance between the detection port and the cameras is fixed to be about 3 times the diameter of the detection port (He et al. 2012).

The ambient temperature of the optical laboratory was controlled around 20° C. The cooling temperatures of the Marana sCMOS and iKon-L 936 CCD cameras were set at -45 ° C and -80 ° C, respectively. Bias and flat images are reduced with Solis, which is camera control software developed by Andor Technology PLC.

A region of [600:1400, 600:1400] is used to calculate the mean value and the variance of counts to make a PTC[3]. The PTC of the sCMOS camera in the 12-bit setting is plotted in Figure 4. The PTC has a sharp drop when pixel counts, as measured in analog to digital units (ADU), are around 3700. When the pixel counts exceed this value, it becomes harder to estimate the number of photons collected accurately. In general, the PTC represents a sensitive tool for evaluating the FWC. FWC is the largest

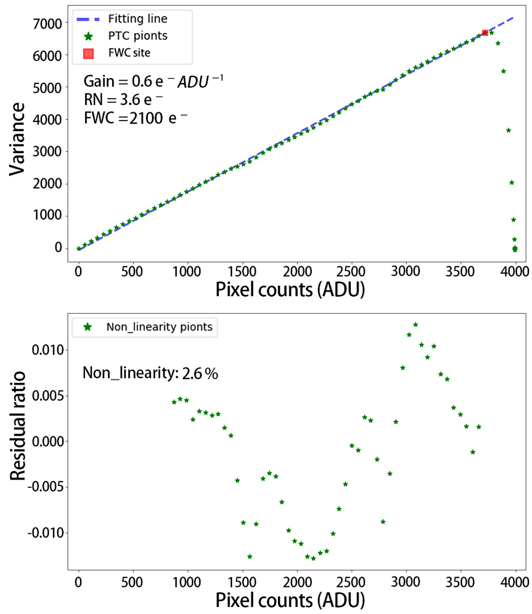

Fig. 4 (*Top*) PTC of Marana sCMOS camera in the 12-bit setting. (*Bottom*) Residual ratio of the sCMOS camera. A range from 20% of saturation to FWC site is applied.

charge a pixel can hold before saturation which results in degradation of the signal. The FWC site means a count level corresponding to FWC in this paper. We obtained values of the gain, RN and FWC of the sCMOS camera in the 12-bit setting of 0.6 e^- ADU^{-1}, 3.6 e^- and 2100 e^-, respectively.

To evaluate nonlinearities in the PTCs of the two cameras, we fitted variance values of the measured samples with a linear function, $Y'(x)$. Here, a residual ratio at each count is defined as follows,

$$Residual = \frac{Y_{\rm n}(x_{\rm n}) - Y'_{\rm n}(x_{\rm n})}{Y'_{\rm full}} \quad (1)$$

where $Y_{\rm n}(x_{\rm n})$ stands for a variance value of a count x_n in the PTC, $Y'_{\rm n}(x_{\rm n})$ means a variance value of x_n in the

[3] The calculation method refers to the *findgain* task command in IRAF.

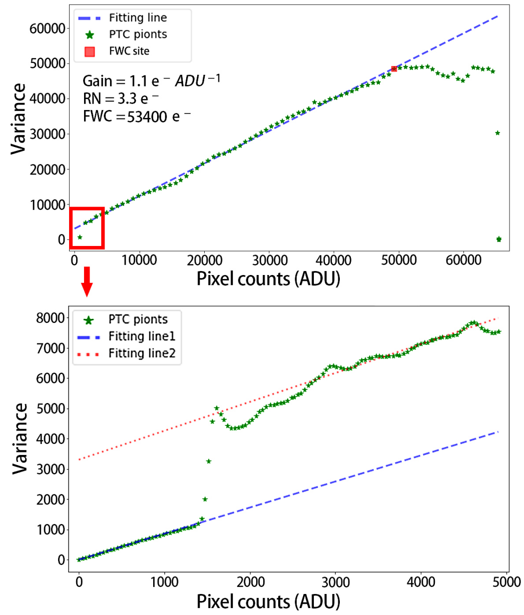

Fig. 5 (*Top*) PTC of the Marana sCMOS camera in the 16-bit setting. A sudden change of variance is seen around 1500 counts. (*Bottom*) Magnified view of the PTC in the lower count range.

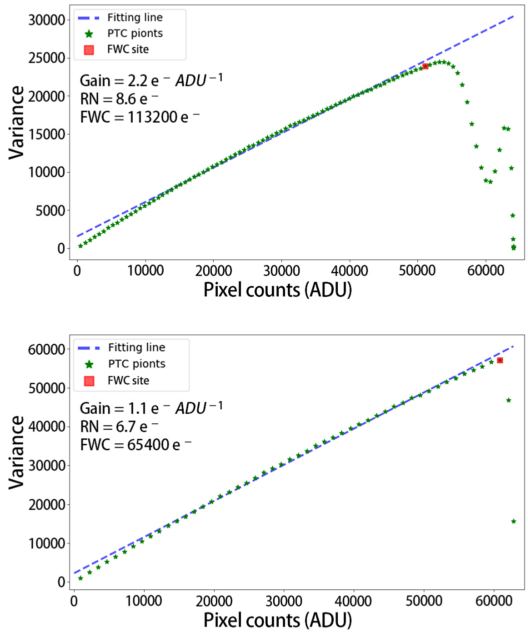

Fig. 6 (*Top*) PTC of the iKon-L CCD camera in the 1 MHz $2\times$ setting. (*Bottom*) PTC of the iKon-L CCD camera in the 1 MHz $4\times$ setting. The curves start drastically falling when the pixel counts are around 52 000 and 60 000, respectively.

$Y'(x)$ and $Y'_{\rm full}$ indicates the value of FWC in the PTCs. A peak-to-peak value of the derived residual ratio displayed in Figure 4 is defined as a PTC's nonlinearity. When input light is faint, the PTC's nonlinearities of the sCMOS and CCD cameras are degraded because the RN is dominant. When close to saturation, degradation of the performances could be caused by amplifier circuits in an image sensor and readout circuits in the camera module. A range from 20% of the saturation to the FWC site is applied to evaluate the sensor performances. As shown in Figure 4, the PTC's nonlinearity of the sCMOS camera in the 12-bit setting is 2.6%.

The PTC of the sCMOS camera in the 16-bit setting measured in the same conditions is featured in the top panel of Figure 5. We can ascertain that the gain, RN, FWC and PTC's nonlinearity of the sCMOS camera in the 16-bit setting are 1.1 e$^-$ ADU^{-1}, 3.3 e$^-$, 53 400 e$^-$ and 7.2%, respectively.

The PTC of the CCD camera in the 1 MHz $4\times$ setting obtained with the same methods is displayed in the bottom panel of Figure 6. The curve starts drastically falling when pixel counts are around 58 000. The gain, RN, FWC and PTC's nonlinearity are derived to be 1.1 e$^-$ ADU^{-1}, 6.7 e$^-$, 65 400 e$^-$ and 3.0%, respectively.

Remarkably, the PTC of the sCMOS camera in the 16-bit setting has a sudden change in a lower count range as seen in the top panel of Figure 5. The PTC produced by a series of lower count images is depicted in the bottom panel of Figure 5. It is clearly seen that a sudden change occurs around 1500 counts and a wavy profile is visible in the range from 1500 to 5000 counts. We checked a reproducibility of the sudden change and the wavy profile of the PTC in the lower count range with three different wavelength light sources at 365 nm, 590 nm and 850 nm and confirmed that the same features are obtained with different light source.

The sudden change seen in the lower count range of the sCMOS camera in the 16-bit setting could be caused by a 12-bit dual-amplifier architecture in the sCMOS camera. Unlike the 16-bit data of the CCD which is sampled by a 16-bit ADC, data from the sCMOS are sampled by both 12-bit high gain and low gain amplifiers simultaneously and the 16-bit image is produced with two 12-bit images, which means that they are not real 16-bit output data. Other problems that this architecture affects are that astronomical observations need to be verified through further laboratory tests and test observations.

The PTC of the iKon-L 936 CCD camera was evaluated with the same methods as the sCMOS. Because the source of RN has been subtracted when evaluating variance values, which refers to the findgain task command in IRAF, the measured variances of the CCD camera are lower than what are expected in a range between 0 and 10 000 ADU as seen in Figure 6. The PTC of the CCD camera in the 1 MHz $2\times$ setting starts drastically falling when the pixel count is around 52 000. The values of

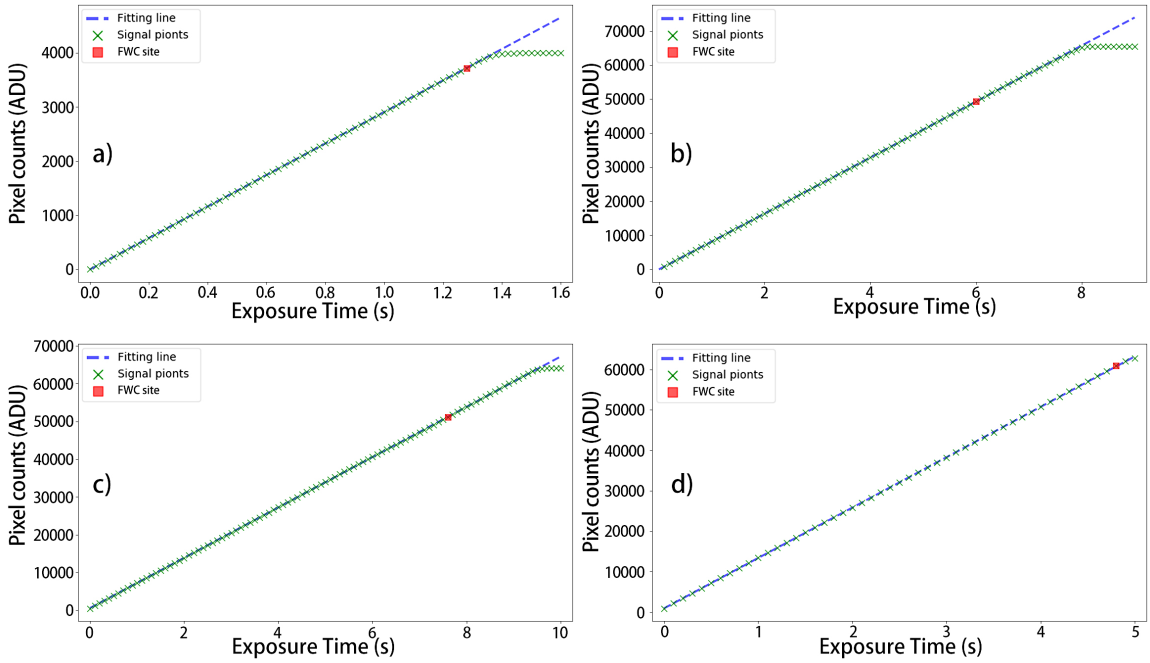

Fig. 7 Linearity curves evaluated in a range from 20% of the saturation to the FWC sites. The top panels are linearity curves of the Marana sCMOS camera in the 12-bit (a) and 16-bit (b) settings. The bottom panels are linearity curves of the iKon-L CCD camera in the 1 MHz 2× (c) and 4× (d) settings. The linearities of the Marana sCMOS camera in the 12-bit and 16-bit settings, and the iKon-L CCD camera in the 1 MHz 2× and 4× settings are 99.7%, 99.7%, 99.5% and 99.7%, respectively.

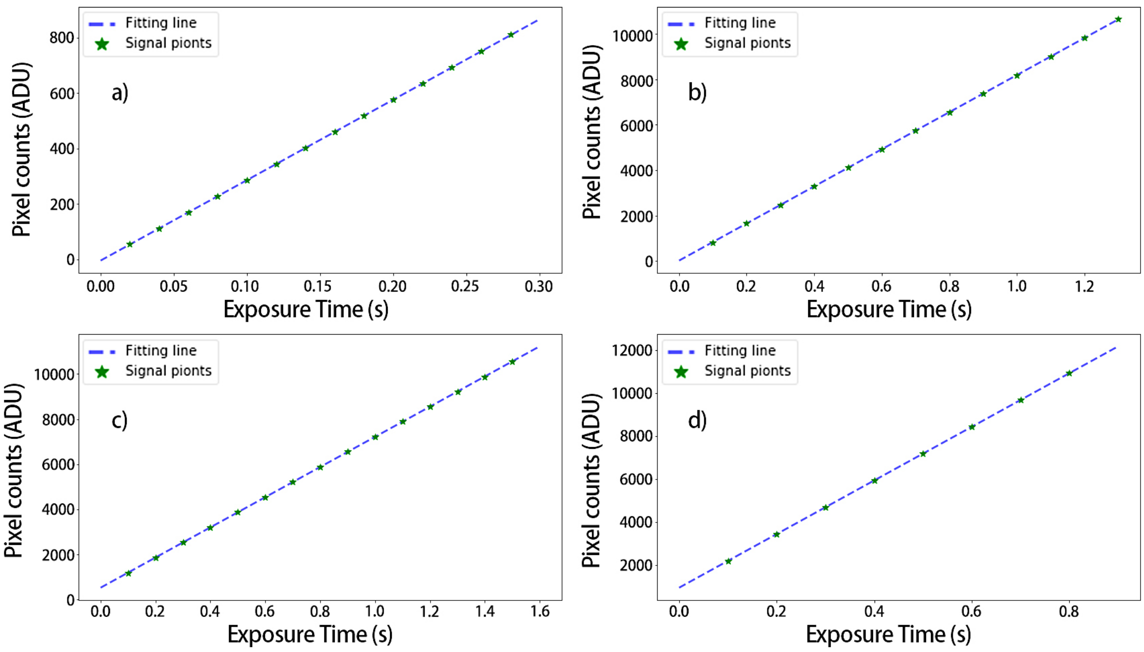

Fig. 8 Linearity curves evaluated in a range lower than 20% of saturation. The top panels are linearity curves of the Marana sCMOS camera in the 12-bit (a) and 16-bit (b) settings. The bottom panels are linearity curves of the iKon-L CCD camera in the 1 MHz 2× (c) and 4× (d) settings. The linearity curves of the Marana sCMOS camera in the 12-bit and 16-bit settings, and the iKon-L CCD camera in the 1 MHz 2× and 4× settings are 98.9%, 97.9%, 98.7% and 99.8%, respectively. The sudden change as seen in the PTC is not confirmed in the linearity curve of the Marana sCMOS camera in the 16-bit setting.

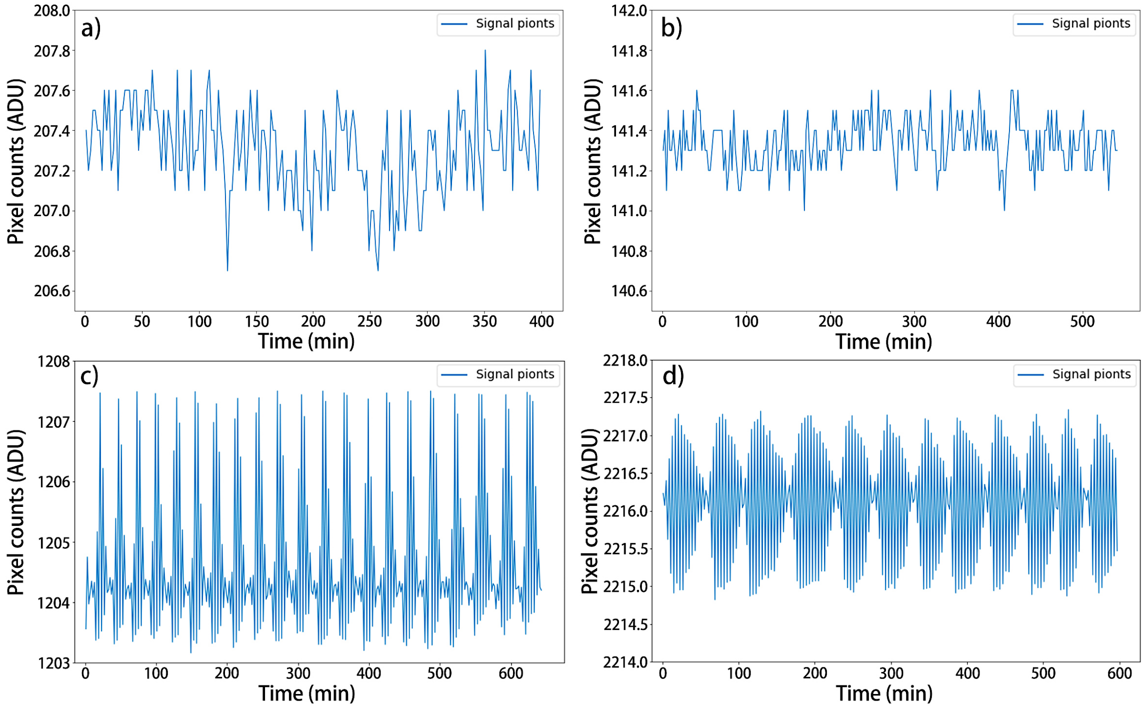

Fig. 9 Time series samples of bias counts of the Marana sCMOS camera in the 12-bit (a) and 16-bit (b) settings, and the iKon-L CCD camera in the 1 MHz 2× (c) and 4× (d) settings. The mean values and standard deviations of the time series data are 207.4 and 0.22, 141.3 and 0.12, 1204.6 and 1.26, and 2216.1 and 0.83, respectively.

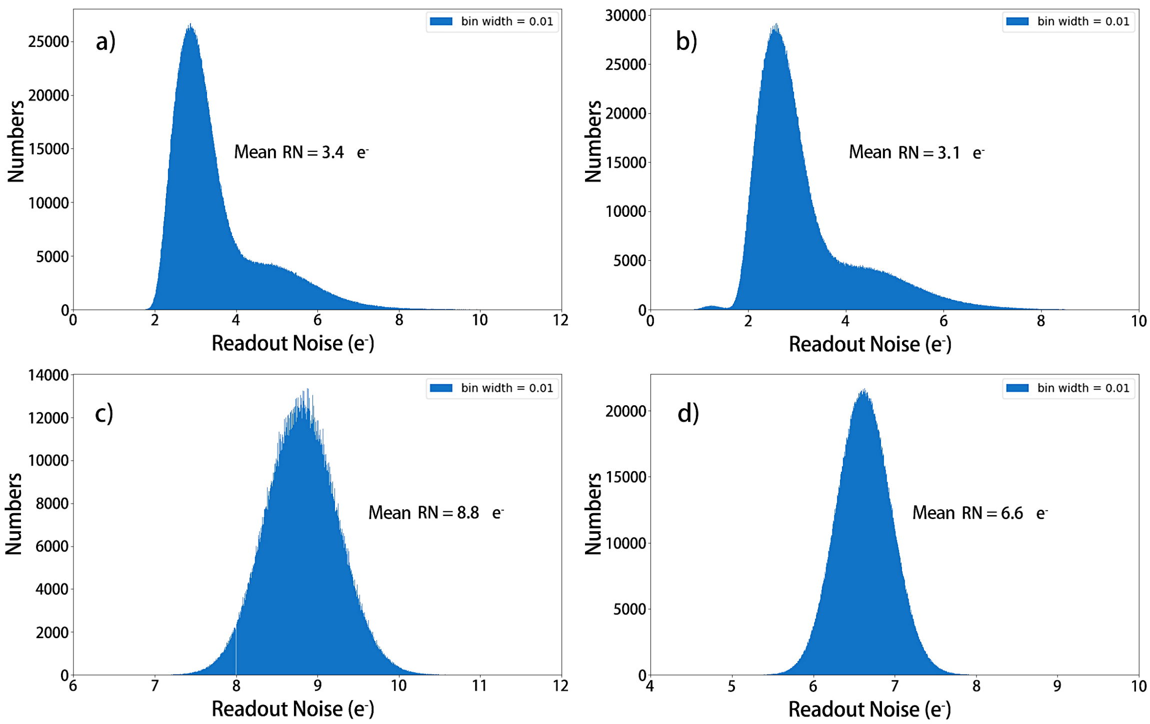

Fig. 10 Histograms of number density of pixel RN measured with the Marana sCMOS camera in the 12-bit (a) and 16-bit (b) settings, and the iKon-L CCD camera in the 1 MHz 2× (c) and 4× (d) settings. The mean values of the pixel RN are 3.4 e^- and 3.1 e^-, 8.8 e^- and 6.6 e^-, respectively.

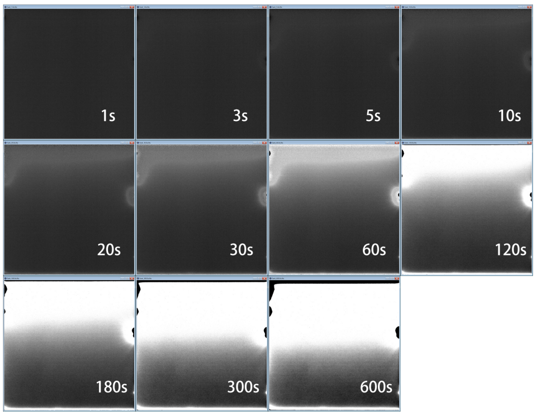

Fig. 11 Changes in dark images obtained with the Marana sCMOS camera in the 12-bit setting shown with the same displayed range. There are bright spots at edges of the frame which become brighter with longer exposure time.

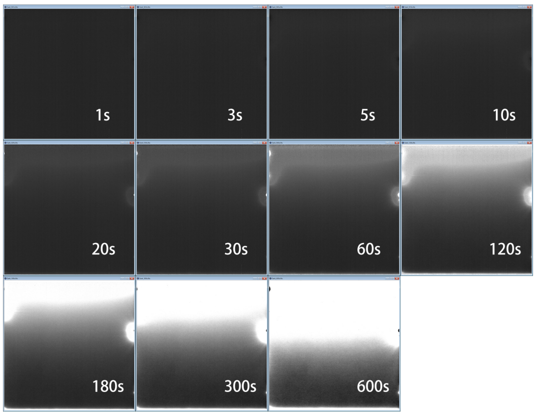

Fig. 12 Dark images taken with the Marana sCMOS camera in the 16-bit setting. Counts in spots become larger with longer exposure time.

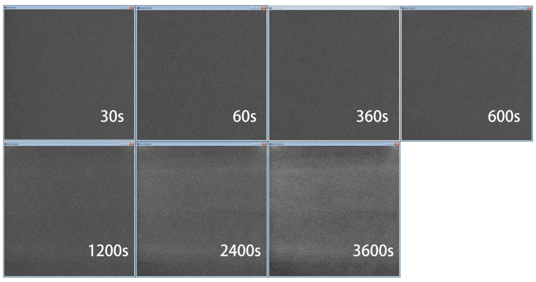

Fig. 13 Dark images taken with the iKon-L CCD camera in the 1 MHz 2× setting. There are no spots or glow in the CCD images.

gain, RN, FWC and PTC's nonlinearity are derived to be 2.2 e^- ADU^{-1}, 8.6 e^-, 113 200 e^- and 4.6%, respectively.

3.2 Linearity

The linearity of photon response is evaluated by plotting signal as a function of exposure time. The linearity value is percentage deviation from ideal linearity over dynamic range. In order to characterize the linearity of the image sensors, a series of flat images was taken with increasing exposure time until reaching saturation. A region of [600:1400, 600:1400] is chosen to evaluate the linearity of the sCMOS and CCD cameras. The linearity curves measured with the sCMOS camera in the 12-bit, 16-bit and the CCD camera in the 1 MHz 2× and 4× settings are plotted in Figure 7.

Same as in Section 3.1, a range from 20% of the saturation to the FWC site derived from the PTC is chosen to evaluate the linearity of the two cameras. The linearities of the sCMOS camera in the 12-bit and 16-bit settings, and the CCD camera in the 1 MHz 2× and 4× settings are 99.7%, 99.7%, 99.5% and 99.7%, respectively.

Because faint astronomical objects generate lower output signals, we evaluated linearities in a range lower than 20% of the saturation as displayed in Figure 8. The linearities in the lower range of the sCMOS camera in the 12-bit and 16-bit settings, and the CCD camera in the 1 MHz 2× and 4× settings are 98.9%, 97.9%, 98.7% and 99.8%, respectively. The sudden change as seen in the PTC is not confirmed in the linearity curve of the Marana sCMOS camera in the 16-bit setting.

3.3 Stability of Bias

The stability of the bias level is essential for ensuring the quality of photometric observations. To evaluate the stability of bias of the two cameras, we took over 200 bias frames with the two cameras in the two different settings every two minutes. Signals from pixels in a region of [600:1400,600:1400] were used to derive time variations of the mean values and standard deviations of pixel counts.

The results are plotted in Figure 9. The mean values and standard deviations of sCMOS 12-bit, sCMOS 16-bit, CCD 1 MHz 2× and CCD 1 MHz 4× were 207.4 and 0.22, 141.3 and 0.12, 1204 and 1.23, 2216 and 0.87, respectively. The results demonstrate that the bias frames of the two cameras in the four different settings are all stable on a 10 hour timescale.

3.4 Statistics of Pixel Readout Noise

In order to evaluate the pixel RN, the 200 bias frames are used to calculate the standard deviation of count values for each pixel.

The histograms of number density of RN for the CCD camera in the two different settings are distributed as a Gaussian function with mean values of 8.8 e^- and 6.6 e^- as displayed in Figure 10. In the histograms for the sCMOS camera in the 12-bit and 16-bit settings, additional components of excess noise are found. We confirmed that

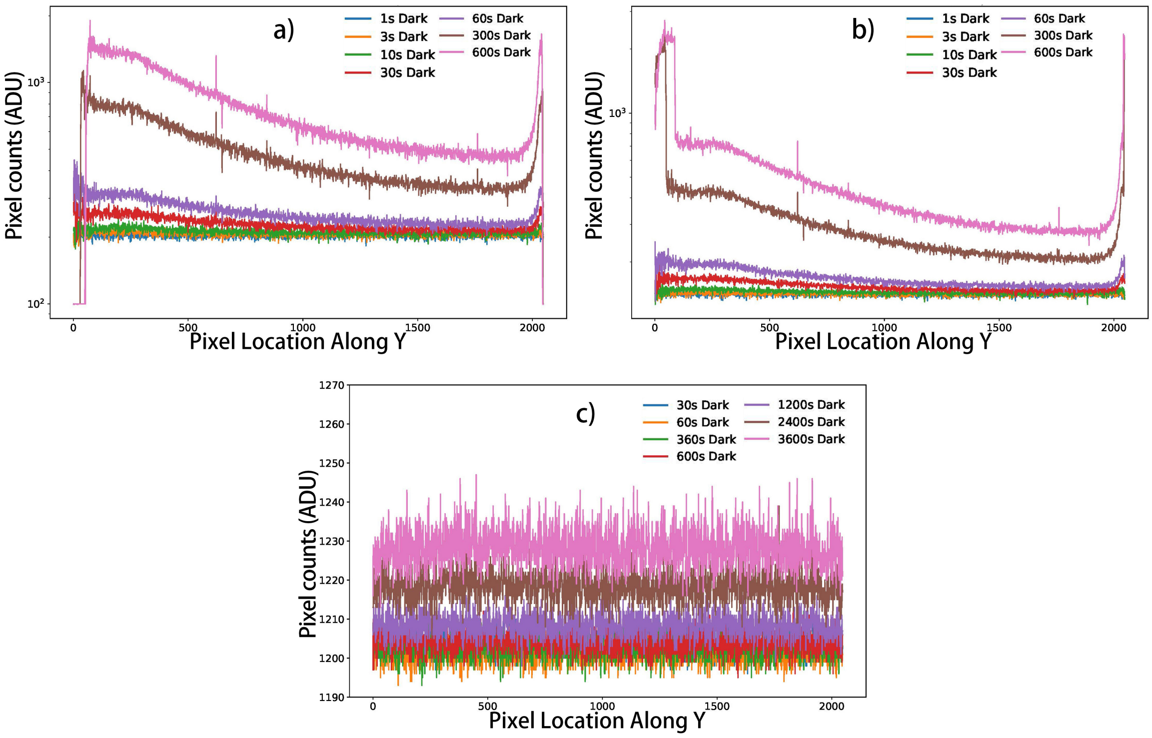

Fig. 14 Distribution of pixel counts along the y-axis at x of 1000 of the Marana sCMOS camera in the 12-bit (a) and 16-bit (b) settings, and the iKon-L CCD camera in the 1 MHz 2× (c) settings. The dark image of the Marana sCMOS camera is not uniform due to the glow.

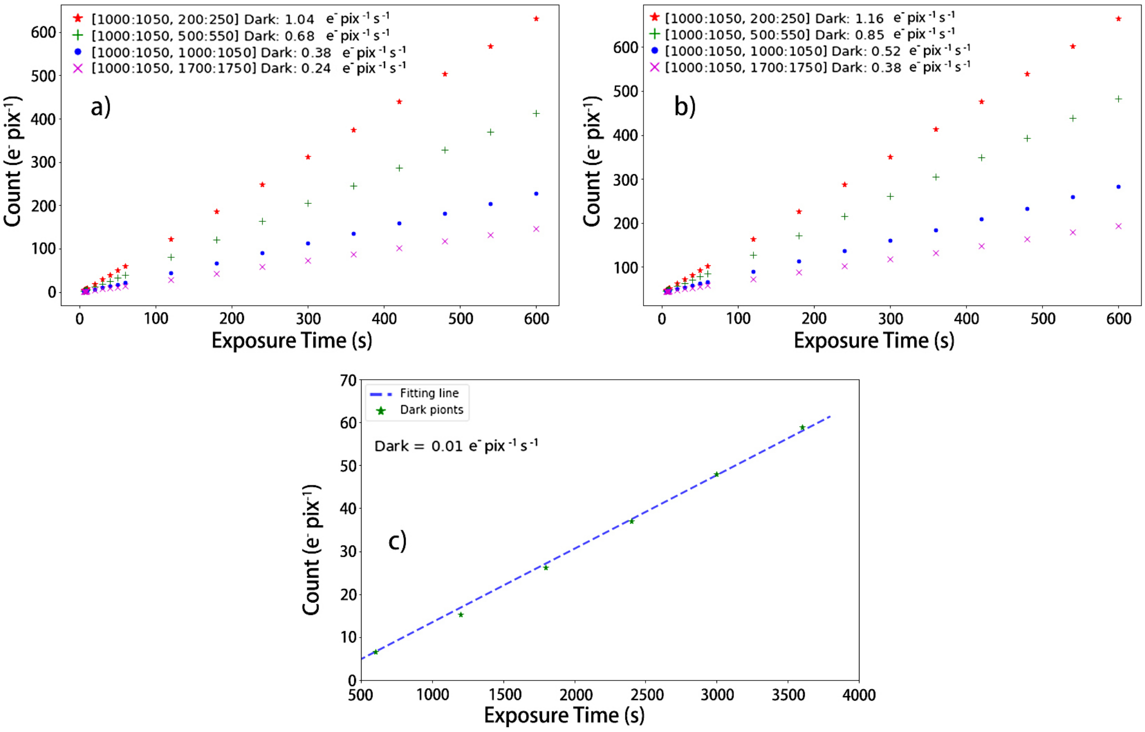

Fig. 15 Time dependences of pixel counts in dark frames obtained with the sCMOS camera in the 12-bit (a) and 16-bit (b) settings and the CCD camera in the 1 MHz 2× setting (c).

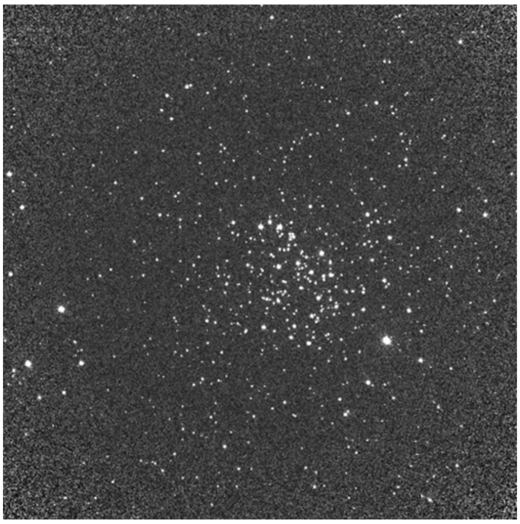

Fig. 16 Open cluster M67 obtained with the sCMOS camera. An FOV of the image is about $38' \times 38'$.

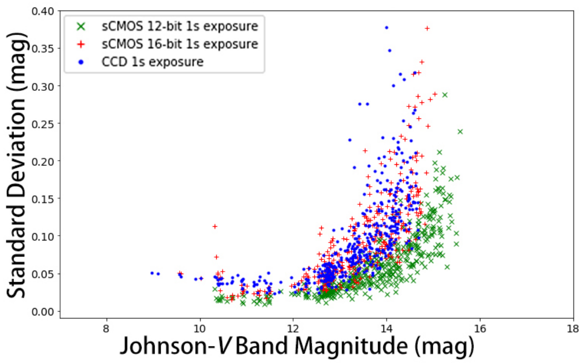

Fig. 17 Photometric stabilities of the M67 sources measured with the *V*-band filter and the sCMOS 12-bit (*green*) and 16-bit (red), CCD 1 MHz 2× (*blue*) settings. The exposure time is 1 s.

pixels with RN values greater than 4.5 e$^-$ are distributed randomly over the whole area in the frame. The mean values of RN are 3.4 e$^-$ and 3.1 e$^-$, respectively.

3.5 Dynamic Range

The dynamic range of a camera is defined as a ratio of the FWC to the RN values, corresponding to the largest signal to noise ratio without photon noise. In survey observations in higher stellar density fields, a larger dynamic range is advantageous because more information is recorded.

The dynamic ranges of the sCMOS camera in the 12-bit and 16-bit settings, and the CCD camera in the 1 MHz 2× and 4× settings are calculated to be 568, 16 364, 12 987 and 9159, respectively.

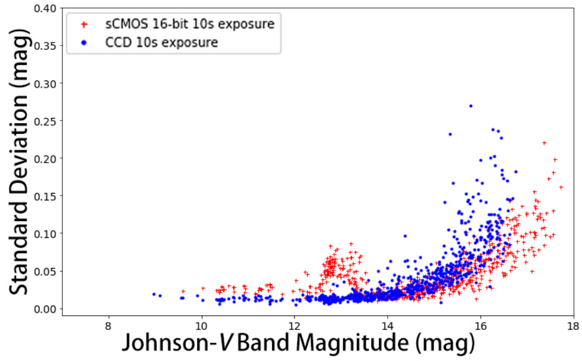

Fig. 18 Photometric stabilities of the M67 sources measured with the *V*-band filter and the sCMOS 12-bit (*green*) and 16-bit (*red*), and CCD 1 MHz 2× (*blue*) settings. The exposure time is 10 s. The photometric stability of the sCMOS camera is degraded by about 6 times in a range between 12.2 and 13.5 mag.

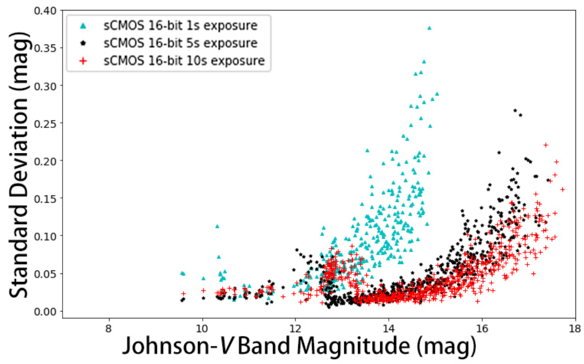

Fig. 19 Photometric stabilities of the M67 sources measured with the *V*-band filter and the sCMOS 16-bit settings. The exposure times are 1 s (*turquoise*), 5 s (*black*) and 10 s (*red*).

3.6 Pixel Nonuniformity

There are different photon responses in pixels when an image sensor is exposed by uniform light. This difference is called pixel nonuniformity, or Photo Response Non-Uniformity (PRNU), which can be collected with the flat reduction method with flat images produced with uniform incident light. The PRNU, $P_{\rm N}$, is evaluated with the following equation,

$$P_{\rm N} = \frac{\sigma_{\rm A}}{\rm Mean(A)} \quad (2)$$

where $\sigma_{\rm A}$ is a standard deviation of pixel counts in the flat image, and Mean(A) is the mean value of pixel counts in the flat image.

The pixel PRNU was evaluated when average signal was approximately 50% of FWC in the central 100×100 region. The PRNU of the sCMOS camera in the 12-bit and 16-bit settings, and the CCD camera in the 1 MHz

2× and 4× settings are 2.51%, 0.24%, 1.19% and 1.24%, respectively.

3.7 Dark current

The dark current arises from self-generated charges without incident light. The dark current affects astronomical observation because excess Poisson noise is generated. It is important to decrease the dark current by cooling down the temperature of the sensor.

The temperatures of the sCMOS and CCD cameras can be cooled down to -45° C and -80° C, respectively. A series of dark images was taken by increasing exposure time captured under dark conditions in the optical laboratory. Three frames were obtained for each exposure time. The dark frames are reduced by the methods of bias subtraction and cosmic ray removal.

Combined dark images of the sCMOS camera in the 12-bit, 16-bit and the CCD camera in the 1 MHz 2× settings are presented with the same displayed range in Figures 11, 12 and 13.

Two spots with larger counts at edges of the frame, corresponding to locations of a high frequency clock pad and a high power consumption buffer, are found in the dark image of the sCMOS camera (Wang et al. 2015). It is noteworthy that the counts in the spots become larger with increasing time and glow with a long exposure time, influencing the surrounding pixels. An engineer at Andor Technology PLC says that an anti-glow technology approach has already been applied to inhibit appearances of the glow.

Projections along the y-axis at x of 1000 are presented in Figure 14. The dark image of the sCMOS camera demonstrates the nonuniformity due to glow.

In order to characterize the dark current and the glow of the sCMOS camera, regions of [1000:1050, 200:250], [1000:1050, 500:550], [1000:1050, 1000:1050] and [1000:1050, 1700:1750] are selected for statistical analysis. The region of [1000:1050, 200:250] is a closer area to the spots. Time dependences of pixel counts of the dark images are displayed in Figure 15. We can deal with image patterns brought by the dark current and glow with the dark correction method. However, influenced by the glow, the issues such as FWC, dynamic range and signal-to-noise ratio are not able to be corrected. The dark current and glow measured with the sCMOS camera in the 12-bit and 16-bit settings in four areas in the frames are listed in Table 2.

At pixels far from the spots, contributions of the glow could be negligible. The dark current of the sCMOS camera in the 12-bit and 16-bit settings are estimated from these regions to be 0.24 e^- pix^{-1} s^{-1} and 0.38 e^- pix^{-1} s^{-1}, respectively.

A central area of [800:1200, 800:1200] is chosen for statistical analysis of the dark current of the CCD camera. The dark current of the CCD camera in the 1 MHz 2× setting was described to be 0.01 e^- pix^{-1} s^{-1}. The temperatures of the sCMOS and CCD cameras are –45° C and -80° C, respectively. We compared the dark currents of the two cameras at their lowest cooling temperatures while the temperatures were not the same. The dark current of the CCD camera is lower than that of the sCMOS camera.

4 FIELD TESTS

We conducted performance tests of the two cameras on a 60 cm telescope at Xinglong Observatory, NAOC. The focal ratio of the telescope is f/4.23. The pixel scales of the sCMOS and CCD cameras are 0.9 and 1.1 arcsec, and fields of view (FOVs) are $30.72' \times 30.72'$ and $37.55' \times 37.55'$, respectively. The typical seeing size at Xinglong Observatory is about 1.8 to 2.0 arcsec, and an image of a point source is extended from 2×2 to 3×3 pixels, satisfying the Nyquist sampling law in the measurements. The 1 MHz 2× setting is selected for the CCD because it has a larger FWC and dynamic range than those of the 4× setting.

The open cluster M67 was observed with the two cameras through a standard Johnson *V*-band filter in photometric conditions.

The photometric stability is defined as the standard deviation of brightness values measured by multiple photometries of the same object. Because the FWC of the sCMOS camera in the 12-bit setting is only about 2057 e^-, a 1 s exposure time was adopted to avoid saturations of bright stars. *V*-band magnitudes of sources in M67 were derived based on reference stars in the SIMBAD database. The standard deviation of the *V*-band magnitudes measured in the multiple observations are shown in Figure 17. The photometric stability is usually limited to be around 1% due to atmospheric scintillation in high-speed observations with exposure times shorter than a few seconds. When the object is bright, the Poisson noise of the object itself is dominant. For comparison with the different settings of the two cameras, the same exposure time is used for the sCMOS camera in 16-bit and CCD camera in 1 MHz 2× settings. The photometric stability of the sCMOS camera is similar to that of the CCD camera as displayed in Figure 17. Considering the mechanical shutter effect of the CCD camera with short exposure times, the sCMOS camera in the 12-bit setting is a better choice for photometry of bright objects with similar brightness that require high frame rates.

Table 2 Dark Current and Glow of the Marana sCMOS Camera in Different Settings

region	12-bit (e^- pix^{-1} s^{-1})	16-bit (e^- pix^{-1} s^{-1})
[1000:1050, 200:250]	1.04	1.16
[1000:1050, 500:550]	0.68	0.85
[1000:1050, 1000:1050]	0.38	0.52
[1000:1050, 1700:1750]	0.24	0.38

The photometric stabilities of the sCMOS camera in the 16-bit setting and the CCD camera in the 1 MHz 2× setting are compared with an exposure time of 10 s to reduce influences of atmospheric scintillation as depicted in Figure 18. In a range between 9 and 14 mag, the standard deviation of brightness magnitudes with the CCD camera is slightly less than that of the sCMOS camera. It is worth noting that the standard deviation values of brightness magnitudes of the sCMOS camera are degraded.

Figure 19 features the photometric stability derived from images with the sCMOS camera in the 16-bit setting with 1, 5 and 10 s exposure time.

By increasing the exposure time, the range in which the photometric stability deteriorates moves toward fainter brightness. These deteriorated ranges correspond to pixel counts between 2400 and 3700 ADU in row images, which are identical to count ranges of the sudden changes seen in the PTCs of the sCMOS camera in the 16-bit setting. Therefore, it is inferred that the pseudo 16-bit data by the dual amplifiers cause worse photometric stability. The exposure time is required to be controlled well to use count ranges except for count values between 1300 and 4000 ADU in the raw images, while the 16-bit setting of the sCMOS camera is utilized in astronomical observations.

5 CONCLUSION

By comparison with the Andor iKon-L 936 CCD camera, the evaluation tests of the Andor Marana sCMOS camera are conducted in the optical laboratory and on the telescope. The results demonstrate that the sCMOS camera has an RN of 3.3 e^-, a high frame rate, a good linearity of 99.7%, a stable bias, a high dynamic range and a good pixel nonuniformity of 0.24% in the 16-bit setting, but lower dynamic range and worse pixel nonuniformity of 2.51% in the 12-bit setting. The dark current of the sCMOS camera in the 12-bit and 16-bit settings is 0.24 e^- pix^{-1} s^{-1} and 0.38 e^- pix^{-1} s^{-1}, respectively. Bright spots at the edges of the frame become brighter with longer exposure time and influence surrounding pixels.

Results of the field tests affirmed that the photometric stabilities of the sCMOS camera in the 12-bit setting are better than those of the CCD camera in the 1 MHz 2× setting. The sCMOS camera in the 12-bit setting could be capable of observing bright objects with similar magnitudes, particularly when high temporal resolution is desired and low dynamic range is acceptable. The pseudo 16-bit data by the dual amplifiers cause worse photometric stability in the range between 2400 and 3700 ADU in raw images. The exposure time is required to be controlled well to use count ranges except count values between 1300 and 4000 ADU in the raw images, while the 16-bit setting of the sCMOS camera is applied in astronomical observations. Consequently, the sCMOS camera is employed for surveys of transients and fast-moving objects that require short exposure times, mostly less than 1 s, and high frame rate. It also meets the requirements of offset guiding due to high sensitivity, high temporal resolution and high stability.

Acknowledgements This work is supported by the National Natural Science Foundation of China (Grant Nos. U1831209, 11803017 and 11903053). We thank Hu Zhan, Xin Zhang, Xiyang Fu and Songling Chen for their kind support in evaluating the performance of cameras. We thank Dawei Xu, Huijuan Wang, Hong Wu, Yinan Zhu, Tianmeng Zhang, Zhou Fan and Juanjuan Ren for helpful discussions. We acknowledge Xiaoming Zhang, Yunpeng Wang and Sen Liu for their help during observing runs.

References

He, Y.-W., Li, P., Wu, H.-P., et al. 2012, Journal of Applied Optics, 33, 548 (in Chinese)

Janesick, J. R. 2007, Photon Transfer DN $\rightarrow \lambda$ (Bellingham, WA USA)

Ma, C., Liu, Y., Li, J., et al. 2015, in Society of Photo-Optical Instrumentation Engineers (SPIE) Conference Series, 9403, Image Sensors and Imaging Systems 2015, eds. R. Widenhorn, & A. Dupret, 940305

Qiu, P., Mao, Y.-N., Lu, X.-M., et al. 2013, RAA (Research in Astronomy and Astrophysics), 13, 615

Wang, X., Ma, C., Liu, Y., et al. 2015, In Proceedings of the International Image Sensor Workshop,